

Acquisition geometry requirements for generating virtual-source data

KURANG MEHTA and ROEL SNIEDER, Colorado School of Mines, Golden, USA

RODNEY CALVERT and JONATHAN SHEIMAN, Shell International Exploration and Production, Houston, USA

Using model and field data, this article reviews the virtual-source method and its acquisition geometry requirements. Before we go into the details of the acquisition geometry requirements, let us briefly review the basic concept and the advantages of the virtual-source method. A typical surface seismic experiment has sources on the surface to excite waves that propagate through the subsurface. Surface receivers record the reflected waves. In order to image the subsurface, we migrate the reflected wavefield recorded by the receivers, using an estimate of the subsurface velocity model. However, the near surface is usually complex, and the velocity is difficult to estimate. These near-surface inhomogeneities, if not represented in the migration velocity model, defocus the deeper image. In order to avoid the estimation of the near-surface velocity model, Bakulin and Calvert (2006) proposed the virtual-source method, a technique that uses cross-correlation of the wavefield recorded by a given pair of receivers to estimate the response between them.

Virtual-source method. Application of the virtual-source method for imaging and time-lapse monitoring below the near-surface overburden requires sources on the surface and receivers below the near-surface, time-varying overburden. Figure 1 depicts the application of the virtual-source method. For the geometry depicted in Figure 1a (sources S1, S2, S3 on the surface and receivers R1 and R2 in the subsurface), Figures 1b and 1c show the receiver gathers corresponding to R1 and R2, respectively. The trace depicted by S1R1 is the wavefield recorded by receiver R1 excited by source S1. A similar notation holds for other traces.

The two receiver gathers when cross-correlated pairwise, create a correlation gather (Figure 1d). Horizontally summing the correlation gathers creates a new trace (Figure 1e) that approximates a signal that would have been recorded at receiver location R2 as if a source were excited at receiver location R1. Figure 1f depicts this virtual source location as VS. Since there is no physical source at the location of R1, the method is known as the *virtual-source method*. Hence, by cross-correlation and summing, we redatum the data down to the receiver locations without knowledge of the overburden velocities.

Figure 1 shows generation of a virtual-source trace by summing the correlation gather over three sources. Theory, however, states that cross-correlation provides the true response between the virtual source and a receiver provided that a continuous distribution of physical sources surround the receivers, as shown in Figure 2a. The triangles A and B depict the receivers, and the dots show the sources. Figure 2b shows the virtual-source data generated after cross-correlation and summing (similar to Figure 1e). For a homogeneous model with velocity c and receivers A and B separated by distance d , cross-correlation and summing results in a nonzero signal for positive and negative times, and, hence, the virtual-source data contain a causal and an acausal pulse arriving at times $\pm c$. The causal pulse refers to the signal recorded by receiver B as if a virtual source at receiver A is excited at time $t=0$ and propagates forward in time. The acausal pulse refers to the signal recorded by

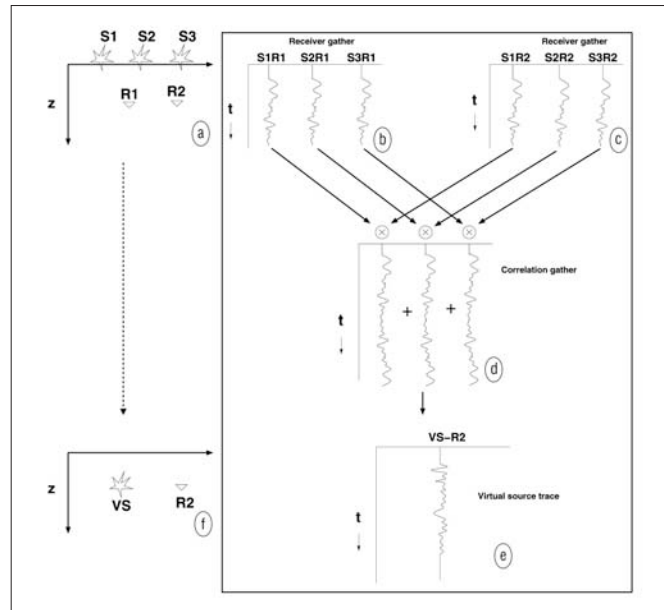


Figure 1. Processing steps for generating a virtual source. (a)=a seismic experiment with surface shooting and subsurface recording. After cross-correlating the receiver gathers (b) and (c) and summing the correlated data (d) over the sources, the resultant trace (e) represents the signal recorded by receiver R2 as if there were a virtual source (VS) at the location of receiver R1 (f).

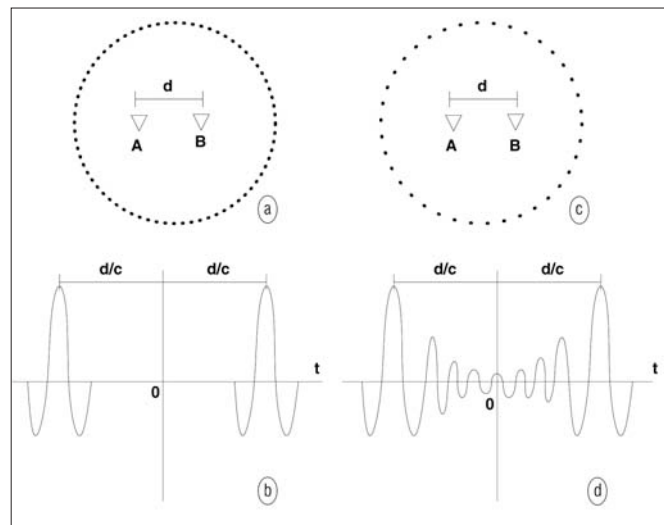


Figure 2. Cartoon of a homogeneous model (velocity = c) with two receivers, A and B, enclosed by sources depicted by dots. For densely spaced sources (a), the response obtained after cross-correlating the wavefield recorded by receivers A and B and summing the correlated data over all the sources (b) is equivalent to putting a physical source at receiver A and recording at receiver B or vice versa. For sparsely spaced sources (c), apart from the causal and acausal responses, the correlation response contains ringing that corresponds to the spatial aliasing.

receiver A as if a virtual source at receiver B is excited at time $t=0$ and propagates backward in time (Petrashen and

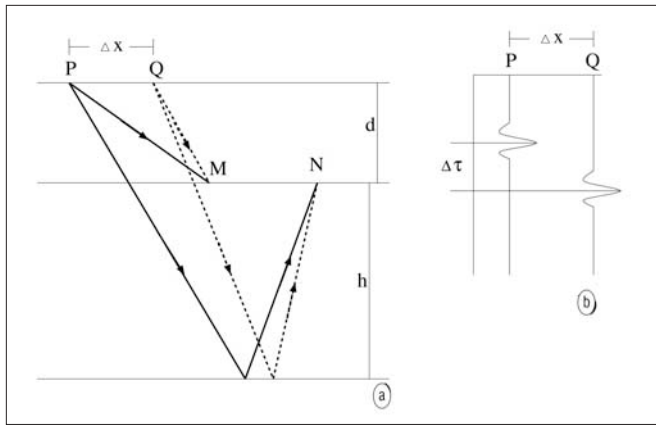


Figure 3. Geometry (a) with two sources, P and Q , on the surface, two receivers, M and N , at depth d and a reflector at depth $d+h$. The paths of propagation from P and Q to M and N are shown by solid and dashed lines, respectively. (b) Two traces (corresponding to the shots at P and Q) of the correlation gather for receivers M and N .

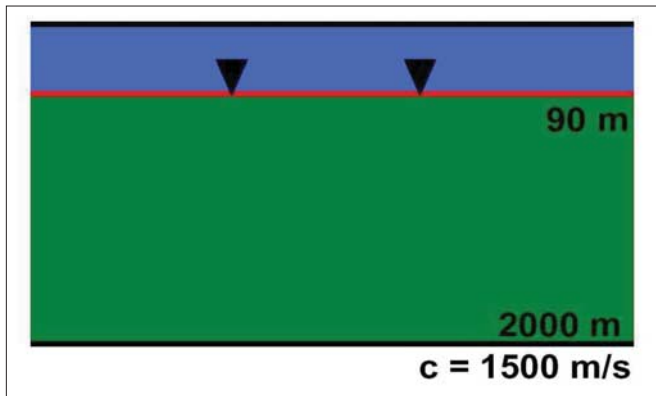


Figure 4. Cartoon showing the geometry for the synthetic model.

Nakhamkin, 1973).

The spacing of the physical sources is a crucial consideration because we cannot have a continuous surface source distribution as required by the theory. If the source spacing is sparse (Figure 2c), the virtual source data (Figure 2d) contain artifacts caused by spatial aliasing in the form of ringing, along with the desired response. This form of spatial aliasing is similar to the aliasing during migration because of sparse receiver spacing. In the next section, we use synthetic models to demonstrate the use of the correlation gather and its $f-k$ domain representation to detect spatial aliasing. We also present, using similar synthetic models, the dependence of the maximum allowable source spacing on the velocity of the subsurface and the source-receiver geometry to prevent spatial aliasing.

The geometry of Figure 2a is an unachievable idealization for geophysical applications. One practical limitation is that, unlike the idealized geometry of sources surrounding the receivers, for geophysical applications we have sources only on one side (i.e., above) the downhole receivers. In a later section, we use Mars Field OBC data to demonstrate the generation of the virtual-source gather and address the ramification of having a finite source aperture.

Maximum allowable source spacing. As illustrated in Figure 2, source spacing is an important consideration while generating virtual-source data. In order to demonstrate the

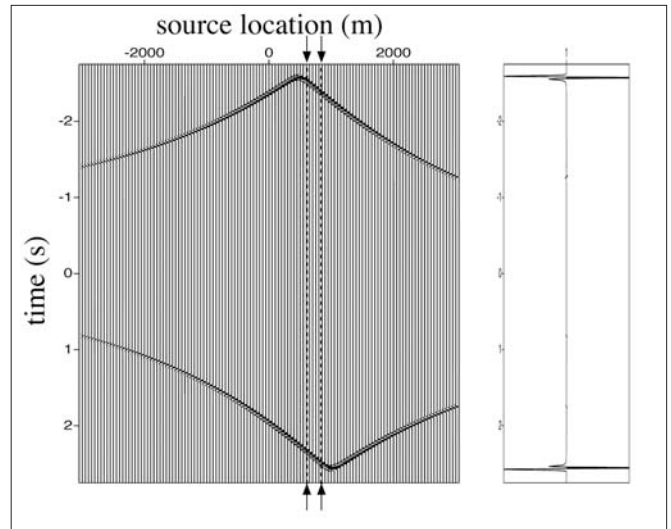


Figure 5. The correlation gather showing the reflection response for the synthetic model with sources every 5 m. Arrows depict the receiver locations in the lateral direction.

usefulness of the correlation gather to detect spatial aliasing, let us suppose a simple geometry (Figure 3a) with two surface sources P and Q , separated by offset Δx and two receivers M and N recording the waves at a depth d . A reflector is at a depth $d+h$. Since we use the reflected wavefield for migration, we focus on the reflection events. To obtain the reflection response between receivers M and N , we cross-correlate the direct arrival from a given shot (say P or Q) recorded by receiver M and the reflection response recorded by receiver N (the raypaths are shown by the arrows in Figure 3a). Figure 3b idealizes the traces in a correlation gather. The trace labeled P is the cross-correlation of the direct arrival due to source P recorded at receiver M and the reflection response caused by source P recorded at receiver N . Similarly, trace Q is the cross-correlation of the direct arrival caused by source Q recorded at receiver M and the reflection response caused by source Q recorded at receiver N . The summation of the traces in the correlation gather provides a trace containing the reflector's reflection as if the source were at M and receiver at N , or vice versa.

Each cross-correlation trace shows a pulse arriving at different times. The arrival time of the pulse for each trace in the correlation gather is equal to the difference in the traveltimes for the waves to propagate from the corresponding source to the two receivers, for example the traveltime difference between the direct arrival P to M and the reflected arrival, P to N .

As will be evident, a larger slope in the correlation gather makes the correlation gather more vulnerable to spatial aliasing. The ratio of the difference in the arrival times of the pulses in the two traces ($\Delta\tau$) and the offset between the two sources P and Q (Δx) gives the slope ($\Delta\tau/\Delta x$) of the reflection response in the correlation gather. For a fixed-source spacing, the maximum slope of the reflection event in the correlation gather is proportional to the difference in the arrival times for adjacent sources and, thus, depends on the velocity of propagation, depth of the receivers (d), depth of the reflector ($d+h$), and the angles of incidence and reflection. For small $\Delta\tau$, the slope of the reflection response is small and, hence, we can have sources far apart without introducing spatial aliasing. A higher maximum slope of the reflection event in the correlation gather, however, requires smaller source spacing to prevent spatial aliasing.

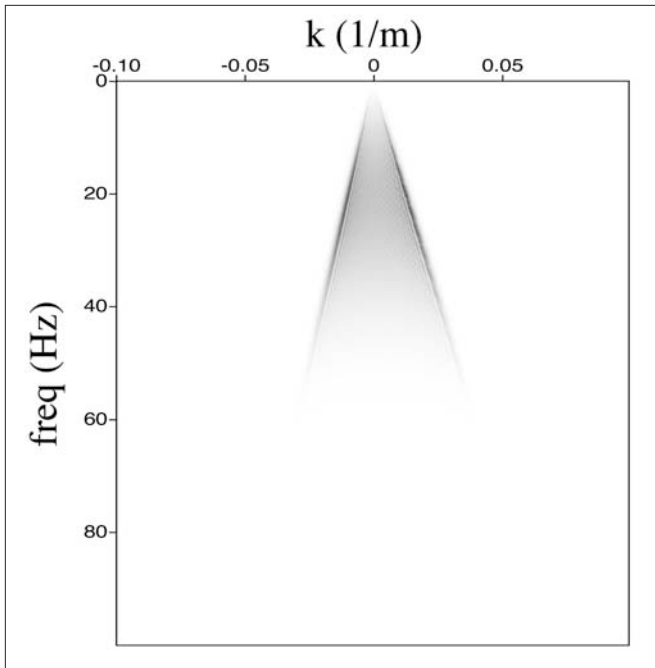


Figure 6. The frequency-wavenumber (f - k) plot corresponding to the correlation gather shown in Figure 5.

Aliased and nonaliased models. We now illustrate the use of the correlation gather and its f - k domain representation to detect spatial aliasing, using a synthetic homogeneous model with two receivers at a depth of 90 m, a single reflector at a depth of 2000 m and velocity 1500 m/s (Figure 4). The physical sources are fired from the surface. The left panel of Figure 5 shows the correlation gather for the model in Figure 4 with 1200 sources spaced every 5 m. The horizontal axis extends from -3000 m to 3000 m ($1200 \times 5 = 6000$ -m source aperture). The two sets of arrows on the horizontal axis depict the location of the two receivers in the lateral direction (500 m and 1000 m). Each trace represents, for a given source location, the cross-correlation of the direct arrival recorded at one receiver with the reflected waves recorded at the other receiver.

The cross-correlation when summed over the physical sources (right panel of Figure 5) gives the causal and acausal reflection events, similar to the causal and acausal pulses in Figure 2b. The nonzero amplitudes in the horizontal summation of the cross-correlation traces come from the source location where the correlation gather traces (left panel of Figure 5) reach an extremum in arrival time; the arrivals at other source locations interfere destructively. Mathematically, sources located at an extremum in a correlation gather are referred to as stationary phase contributors or stationary sources (Wapenaar, et al., 2005; Snieder, et al., 2006).

For Figure 3a, the stationary source location corresponds to the source location where raypath QM (or PM) coincides with the initial position of raypath QN (or PN). These stationary source locations lie laterally outside the interval between the two receivers, as shown by the two extrema in the left panel of Figure 5.

The source spacing in the correlation gather (left panel in Figure 5) is 5 m. This source spacing is dense enough to prevent spatial aliasing for the maximum slope of the reflection event in the correlation gather. Figure 6 shows the f - k plot of Figure 5's correlation gather. The f - k plot is symmetric in wavenumber direction because the reflection response in Figure 5 contains symmetrical dips. All wavenumbers are

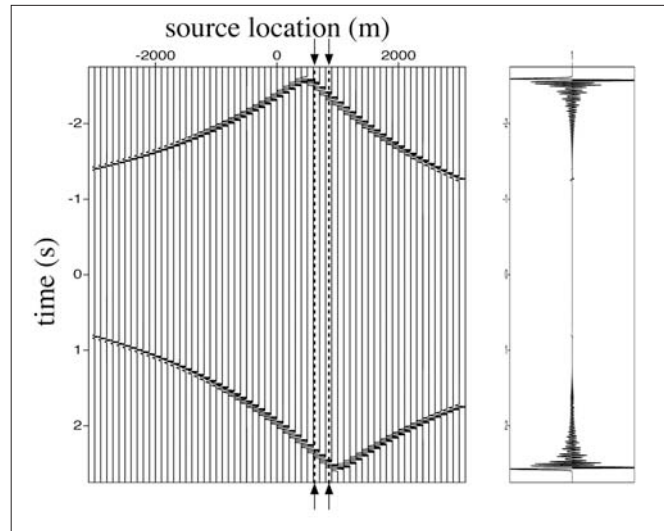


Figure 7. The correlation gather showing the reflection response for the synthetic model with sources every 50 m. Arrows depict the receiver location in the lateral direction.

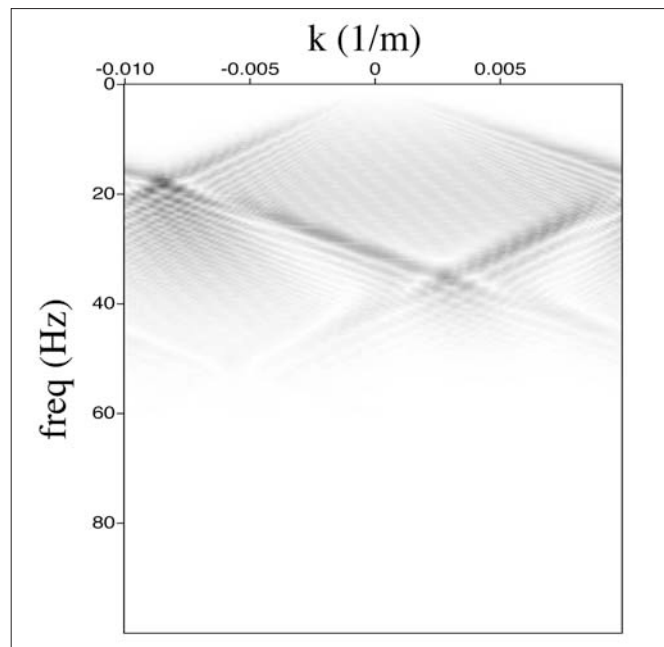


Figure 8. The frequency-wavenumber (f - k) plot corresponding to the correlation gather shown in Figure 7.

within the Nyquist wavenumber range, represented by the limits of the horizontal axis, indicating no spatial aliasing.

The left panel of Figure 7 shows the correlation gather for the same model but now with a source spacing of 50 m, which is sparse for the maximum slope of the reflection event in the correlation gather. This leads to spatial aliasing. The undesired ringing in the horizontal stack (right panel of Figure 7) and the wraparound in the f - k plot (Figure 8) indicate that the data are spatially aliased. For a single reflector case, the combination of correlation gather and its f - k plot is therefore useful for detecting spatial aliasing.

Let us now illustrate the dependence of the maximum allowable source spacing on the velocity of the medium, depth of the receivers (i.e., source-receiver geometry), and the depth of the deepest reflector. Figure 9 shows the correlation gather for velocity of 2000 m/s (instead of 1500 m/s)

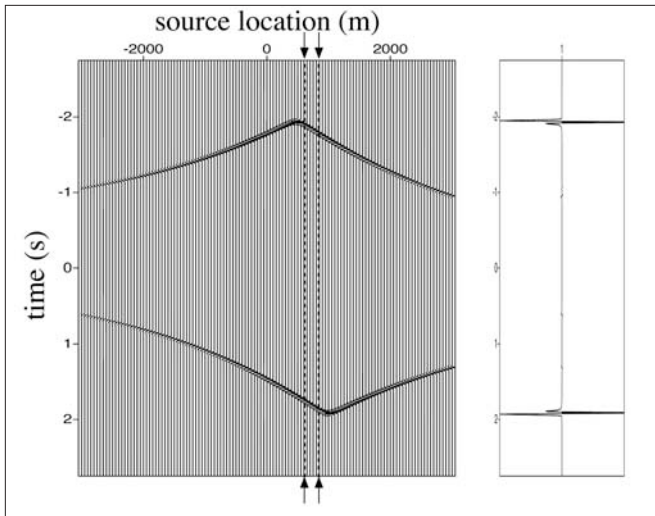


Figure 9. The correlation gather showing the reflection response and horizontal stack for the synthetic model (source spacing 5 m) after increasing the velocity to 2000 m/s. Arrows depict the receiver locations in the lateral direction.

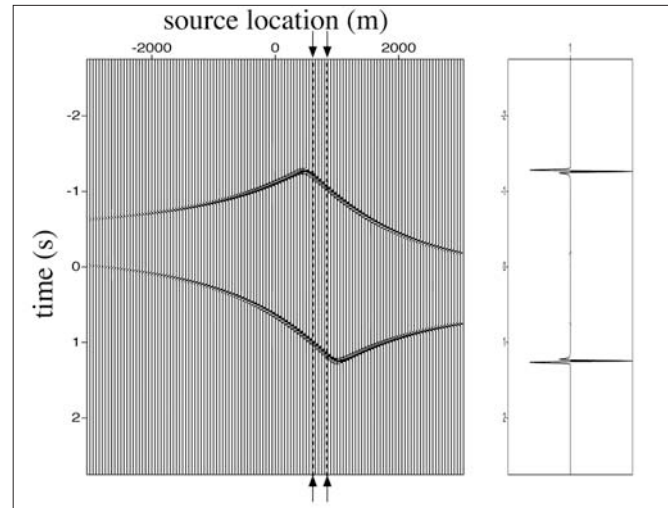


Figure 10. The correlation gather for the synthetic model (source spacing 5 m) after decreasing the reflector depth to 1000 m. Arrows depict the receiver locations in the lateral direction.

with the same model (Figure 4). The maximum slope of reflection event in this correlation gather is smaller as compared to that in the correlation gather in Figure 5. The associated reduction in the travelt ime difference between adjacent receivers with increase in the velocity causes the reduction in the maximum slope of the reflection event. Hence, the maximum slope of the reflection event in the correlation gather reduces with increasing velocity, thus allowing a larger source spacing before encountering spatial aliasing.

The maximum slope of the reflection event in the correlation increases with the reflector's depth, making the reflector depth an important parameter that constrains the maximum allowable source spacing. Figure 10 shows the correlation gather for reflector depth of 1000 m (instead of 2000 m). The velocity of propagation is 1500 m/s and receivers are 90 m deep, as was the case in the initial model in Figure 5. As with the velocity increase, we expect the maximum slope of the reflection event in the correlation gather to decrease with shallower reflector depth because of the diminished travelt ime difference between the adjacent receivers. For the parameters that characterize our synthetic model, this reduction is subtle as compared to the maximum slope of the reflection event in the correlation gather in Figure 5, but in other cases the maximum slope of the reflection event could reduce significantly with decreasing reflector depth. The maximum slope of the reflection event in the correlation gather thus reduces as reflector depth becomes shallower, which increases the maximum allowable source spacing without introducing spatial aliasing.

To illustrate the dependence of the maximum allowable source spacing on the depth of the receivers, starting with the model in Figure 5, we increase the depth of the receivers from 90 m to 1000 m. The left panel of Figure 11 shows the correlation gather for this model with 5-m source spacing, the source spacing of the original model. The maximum slope of the reflection event in this correlation gather is smaller than that in the correlation gather for the original model's shallower receivers. Increasing the depth of the receivers for a fixed-reflector depth is analogous to reducing the depth of the reflector for a fixed receiver depth. Increasing the receiver depth, hence, leads to a decrease in the maximum slope of the reflection event in the correla-

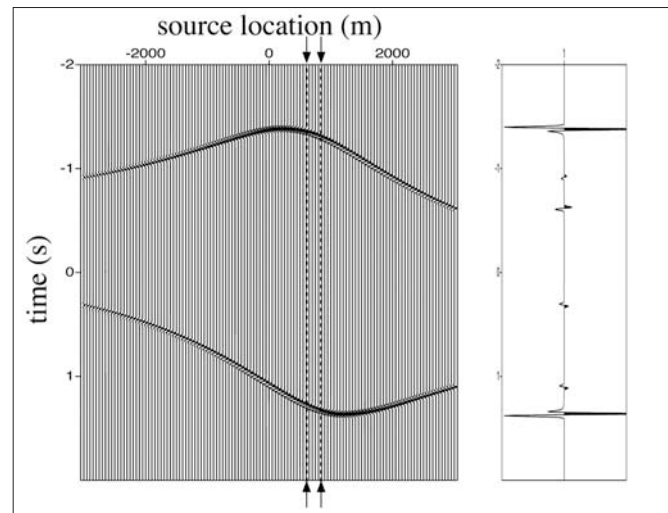


Figure 11. The correlation gather after increasing the receiver depth to 1000 m with sources spaced every 5 m. Arrows depict the receiver locations in the lateral direction.

tion gather. The horizontal stack (right panel of Figure 11) shows the two clean reflections, suggesting that there is no spatial aliasing.

Along with the two reflection events, the horizontal stack of the correlation gather (right panel of Figure 11) also results in four low-amplitude blips. These correspond to the edge effects caused by the contribution of the sources at the ends of the source aperture. The strength of edge effects is inversely proportional to the slope at the ends of the correlation gather. Since the slope of the reflection event at the edges in the correlation gather shown in the left panel of Figure 11 is smaller than that in Figure 5, the edge effects in Figure 11 are stronger than in Figure 5. These edge effects can be suppressed by tapering the ends of the correlation gather before summing. Tapering reduces the trace amplitudes close to the ends in the correlation gather. We illustrate this later in the article.

When the source spacing is increased to 50 m, the resultant horizontal stack (right panel of Figure 12) shows, along with the two reflections and the four low-amplitude blips due to edge effects, weak ringing (around ± 1 s). The weak

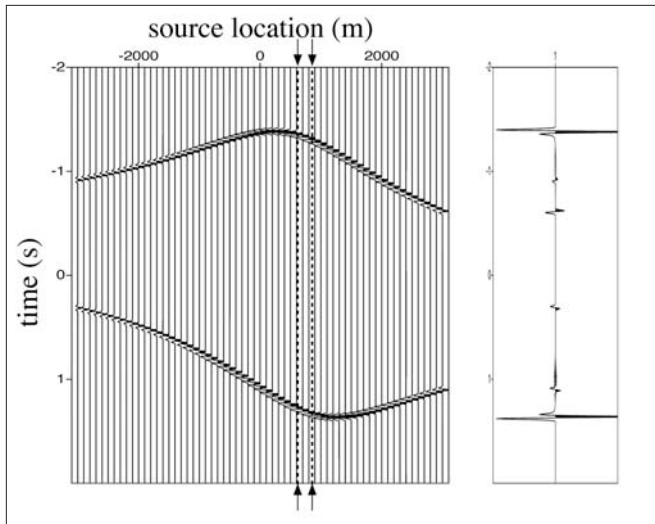


Figure 12. The correlation gather after increasing the receiver depth to 1000 m with sources spaced every 50 m. Arrows depict the receiver locations in the lateral direction.

ringing suggests that the data are spatially aliased but not nearly as severely as for the model with receivers 90 m deep. Deeper receivers therefore allow a larger source spacing without introducing spatial aliasing.

The maximum allowable source spacing to prevent spatial aliasing depends on the velocity, depth of the receivers, and the depth of the reflector. A low-velocity medium with a shallow receiver and deep reflectors requires a denser source spacing to prevent spatial aliasing while generating virtual-source data.

For geophysical applications, we cannot achieve the required source aperture to generate virtual source data. A finite source aperture (sources on the surface and downhole receivers), however, often suffices to generate virtual-source data that agree kinematically, i.e., timing agrees but the amplitudes may not (Mehta et al., 2007a). The next section demonstrates the generation of the virtual-source gather and addresses the ramifications of having only a finite source aperture and the use of the correlation gather to identify the source locations that give a stationary phase contribution.

Generating virtual source gathers. We use the hydrophone component of the four-component sensor permanently placed on the seafloor at the Mars Field. Figure 13 sketches the acquisition geometry. The geometry consists of 364 shots (for our further processing purposes, divided into nine source panels as shown in Figure 13) fired at an interval of 25 m on the sea surface with 120 four-component sensors (spaced every 50 m) permanently placed on the seafloor 1 km deep. Each source panel consists of about 40 shots. The horizontal bar in source panel 7 indicates a gap in the shots due to the presence of the production platform.

For the Mars Field OBC data with receivers placed on the seafloor, the overburden is a homogeneous water layer. Apart from imaging below the complex overburden, the virtual-source method is also a useful tool for time-lapse monitoring, and that is the goal for applying the virtual source method to these data. Changes in the water layer between time-lapse surveys include variations in the sea level, water velocity, and sea surface roughness. Acquisition discrepancies between repeat acquisitions include variations in the shot locations even though seafloor receivers remain fixed. These variations in the water layer and acquisition discrepancies create a problem for seismic monitoring aimed

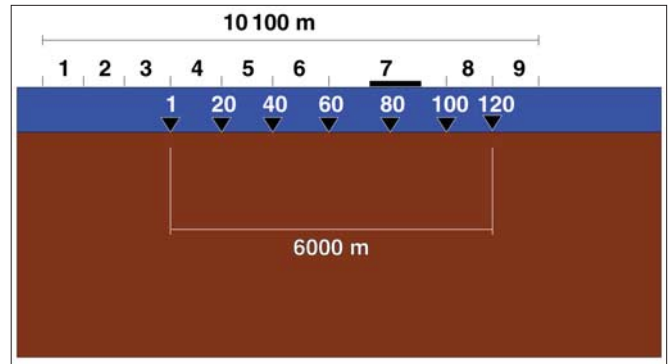


Figure 13. Cartoon of the acquisition geometry of the ocean-bottom cable data obtained from Mars Field. The seafloor is at a depth of 1 km. The 120 four-component sensors permanently placed on the seafloor (indicated by triangles) record the wavefield caused by 364 air-gun shots. The air-gun shots are divided into nine source panels as labeled.

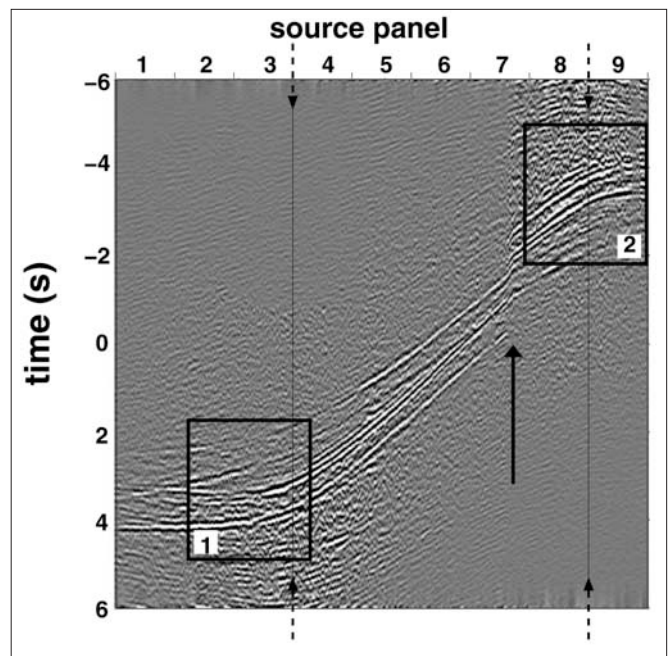


Figure 14. The correlation gather for the hydrophone component generated by cross-correlating the wavefield recorded at receiver 1 with receiver 120. The extrema indicated by boxes 1 and 2 correspond to the sources giving stationary phase contributions. The dashed arrows depict the locations of receivers 1 and 120 in the lateral direction. The solid arrow points to the discontinuity caused by the missing shots in source panel 7.

to detect small time shifts and amplitude changes related to field depletion. The virtual-source method allows us to redatum OBC data by creating virtual-source data at the seafloor receivers without knowing any of above discussed overburden-related, time-varying factors.

The wavefield recorded by a selected reference receiver when cross-correlated with every other receiver and summed over the physical sources creates a virtual-source gather whose traces have a virtual-source location at the reference receiver's location and whose receiver locations are at the locations of the other receivers. The method sketched in Figure 1 creates a single trace (Figure 1e) in a virtual-source gather.

Let us begin by generating virtual-source data with virtual source at receiver 1. To generate the virtual-source trace between virtual-source location 1 and receiver location 120, we stack horizontally the appropriate correlation gather.

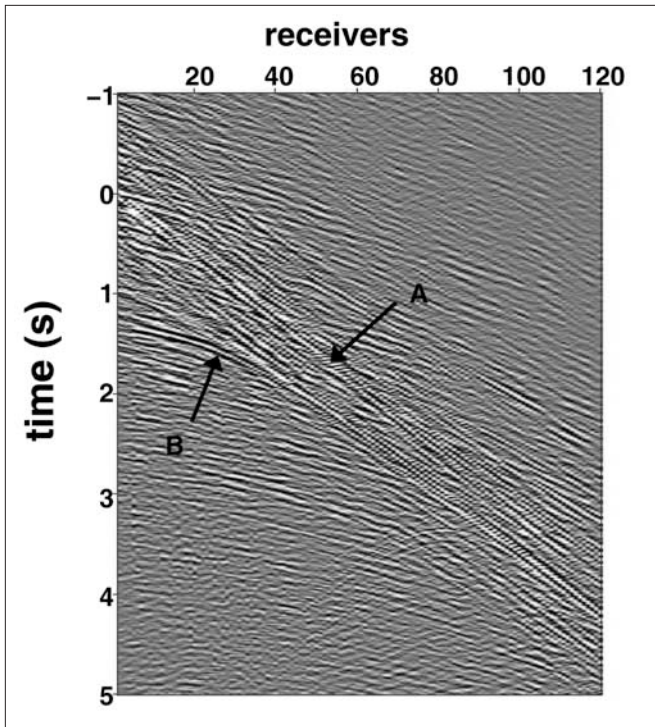


Figure 15. The virtual-source gather with receiver 1 as the virtual source and source panel 1 used for summing. The direct arrival is shown by A, and a strong reflection is shown by B.

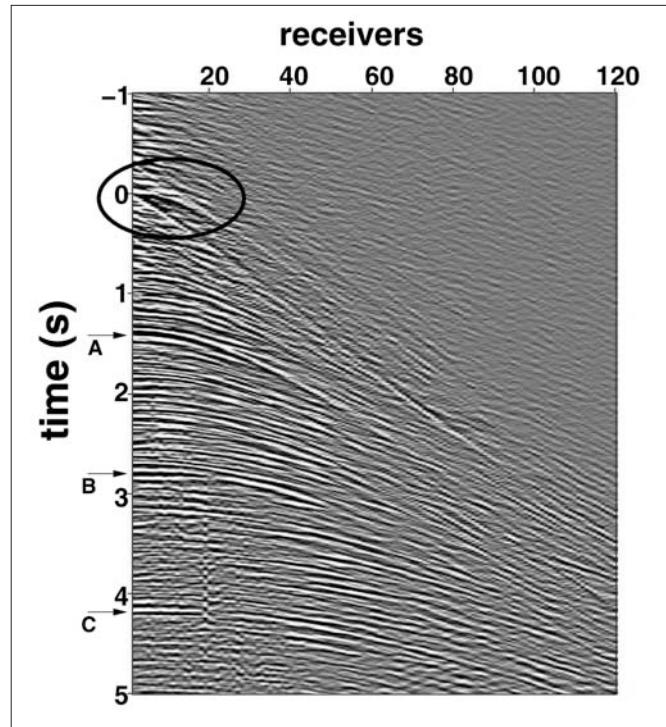


Figure 16. The virtual-source gather with receiver 1 as the virtual source and source panel 3 used for summing. The events indicated by the arrows correspond to the free-surface multiples. An ellipse highlights the artifact caused by the edge effect.

Figure 14 shows this correlation gather with each trace representing the cross-correlation of the entire seismic recording at receiver 1 with that at receiver 120 with each cross-correlation trace corresponding to a different source location. The dashed arrows depict the lateral locations of receivers 1 and 120. The solid arrow indicates a discontinuity in the correlation gather caused by the missing shots in source panel 7. The correlation gather when summed over all the sources creates a trace that represents the wavefield recorded by receiver 120 as if there were a source at receiver 1. Cross-correlating the wavefield recorded by receiver 1 with the wavefield recorded by each other receiver and summing over the sources creates similar virtual-source traces. These virtual-source traces when grouped form a virtual-source gather with virtual source at receiver 1. In the stack of Figure 14's traces, the physical sources laterally located in the stationary region (highlighted by boxes 1 and 2) give nonzero contributions both at positive and negative times; the cross-correlation traces with sources placed at other locations give contributions that interfere destructively.

In order to illustrate the contribution of different sources in the source aperture, we generate a virtual-source gather by summing the correlation gather over sources in a subset of the source aperture. Figure 15 shows the virtual-source gather with receiver 1 as the virtual source and the correlation gathers summed over the sources in source panel 1 only. The gather looks similar to a conventional shot gather. The virtual-source gather shows a direct arrival (A), a few refractions, and a strong reflection (B). Now consider the contributions to a virtual-source gather by sources in source panel 3. In Figure 14, for the positive times, source panel 3 contains the stationary sources (local extrema in the arrival times) for wave propagation between receivers 1 and 120. Similar cross-correlation gathers can be generated to illus-

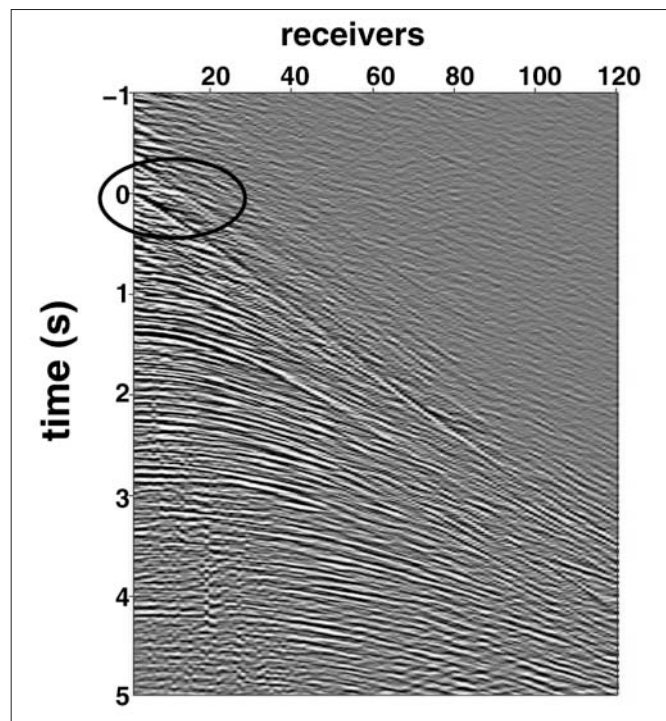


Figure 17. The virtual-source gather in Figure 16 after suppressing the edge effect by applying a linear taper.

trate the wave propagation between receiver 1 and every other receiver. Instead of summing over the sources in source panel 1, the correlation gather, when summed over the sources in source panel 3, gives a virtual-source gather shown in Figure 16. Apart from a few refractions, most of

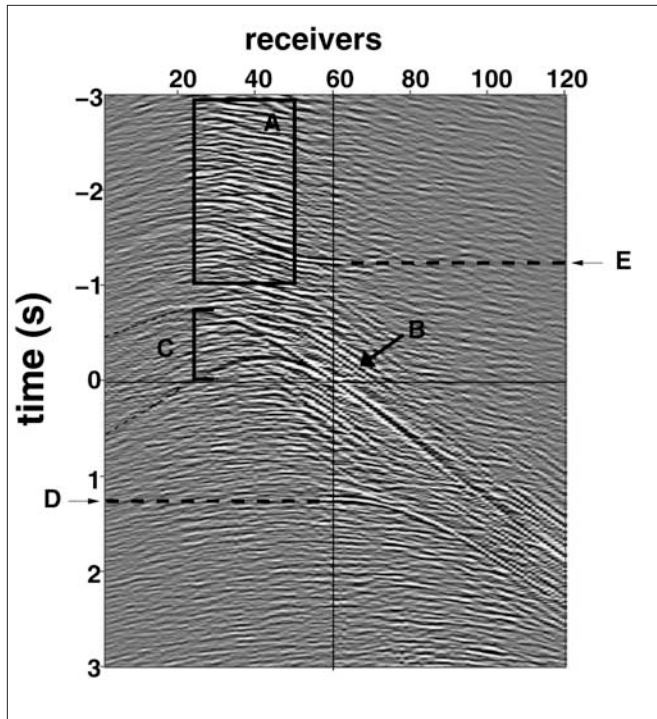


Figure 18. The virtual-source gather with receiver 60 as the virtual source and source panel 5 used for summing.

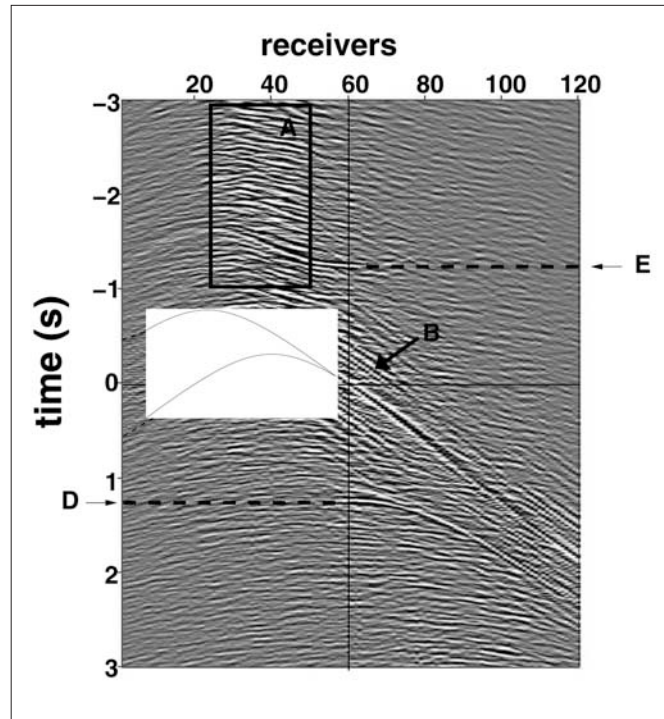


Figure 19. The same virtual-source gather as in Figure 18 with the travel-time difference curves as a diagnostic for the shape of the artifact caused by the edge effect.

the arrivals are reflections. The three strong reflection events occurring at about 1.4, 2.8, and 4.2 s are marked by A, B, and C, respectively. The event close to the direct arrival for near offset, enclosed by an ellipse, is an artifact caused by edge effects associated with the contribution of the sources at the ends of source panel 3. We know that this is edge effect because it is practically suppressed (Figure 17) after applying a linear taper to the ends of the correlation gathers used for generating the virtual-source gather. Note that the slowness of the arrivals in the virtual-source gathers of Figures 15 and 16 are different. The choice of the source panel can thus be used as a filter to select the slowness in the virtual-source gathers.

For further insights in generating a virtual-source gather, consider the virtual-source gather with receiver 60 as the virtual source and the correlation gather summed over the sources in source panel 5 (Figure 18). We begin by generating a virtual-source gather by stacking the correlation gather over a small-source aperture (source panel 5). Using a small source aperture also leads to artifacts in the virtual source gather as we discuss in the following paragraph. To illustrate the effect of increasing the source aperture on the subsurface response and artifacts, we show later in this article (see Figure 21) the virtual-source gather generated with receiver 60 as the virtual source and all the sources used for summing.

In Figure 18, the wavefield for positive times and positive offsets (with respect to receiver 60) is comparable to a conventional shot gather. It consists mainly of the direct arrival, refractions, and a strong reflection (D) at 1.3 s. The negative offset and positive times contain practically no arrivals because we use sources in source panel 5 for summing the correlation gather. Since source panel 5 is located to the left of receiver 60 (Figure 13), waves propagate diagonally from left to right as they arrive at the receiver 60 (virtual source). There is also a reflection (E) at approximately

-1.3 s that corresponds to the acausal part of the reflection response. Box A shows a group of spurious arrivals that arise because the correlation gather is summed over a small subset of sources (source panel 5). When the correlation gather is summed over a small number of sources, the nonstationary phase contribution does not average out and shows up in the virtual-source data. As we will see later, these spurious events average out by using a larger source aperture.

If two traces that are cross-correlated have the same source wavelet, then the cross-correlation produces the autocorrelation of the wavelet. The weak arrivals marked by B have moveout parallel to the strong direct arrival and correspond to the side lobes of the autocorrelation of the source-time function generated when the wavefield recorded at the virtual source location is cross-correlated with the wavefield recorded by the receivers. Trace-by-trace deconvolution of the correlation gather by the autocorrelation of the source-time function (Mehta et al., 2007b) suppresses these side lobes.

The direct arrival extends to negative times to give two spurious arrivals shown by C, which correspond to the edge effect discussed in the previous section. A useful tool to diagnose the shape of the edge effect is the traveltime difference curve. The edge effect is caused by the two sources at each of the two ends of the source aperture (source panel 5). For each of the two end sources, we plot the difference of the traveltimes of the waves to travel from the source to receiver 60 and traveltimes for the wavefield to travel from the same source to the receivers 1 through 59. Hence, we get two curves (one for each end source in the source aperture), which we refer as the traveltimes difference curves. The traveltimes difference curves (Figure 19) for the end sources in source panel 5, using a water velocity of 1500 m/s, agree kinematically (timing agrees but the amplitudes may not) with the artifacts caused by the edge effect. There are two possible ways to suppress the edge effect: taper the ends of

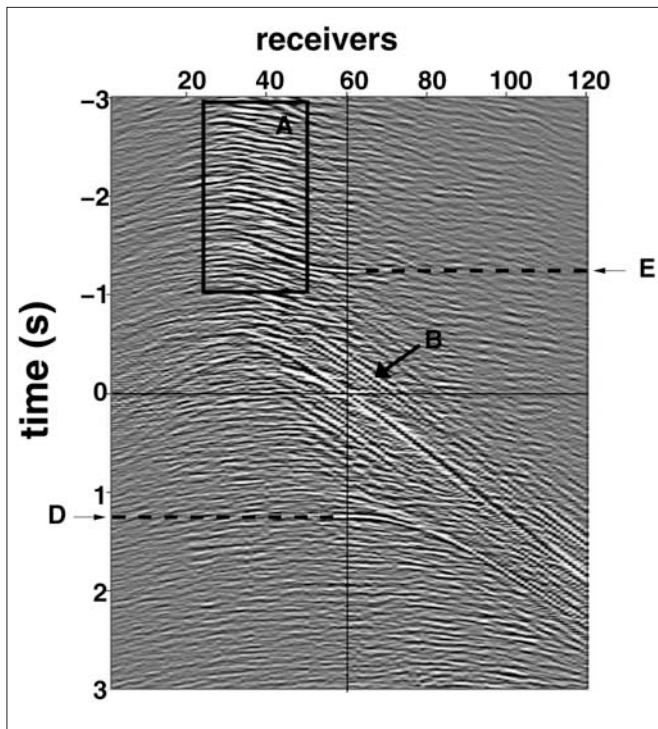


Figure 20. The same virtual-source gather as in Figure 18 after suppressing the edge effect by applying a linear taper.

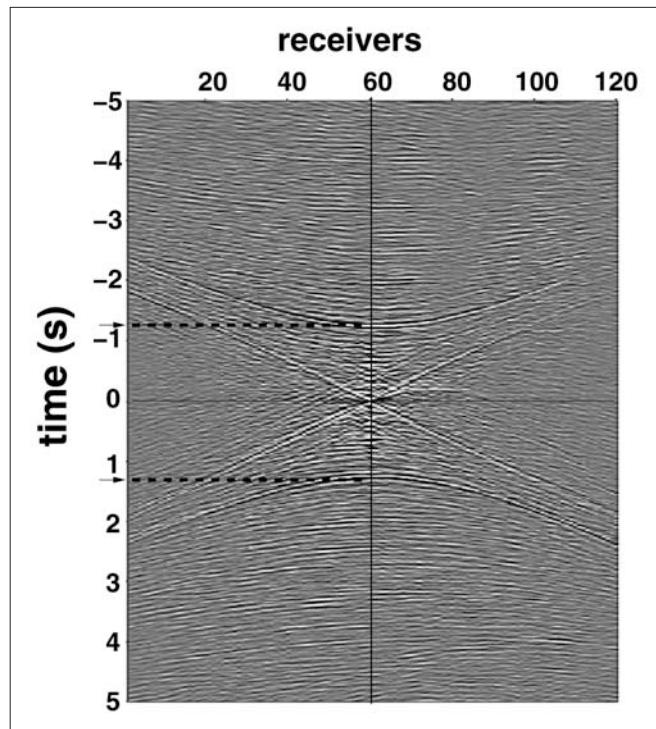


Figure 21. The virtual-source gather with receiver 60 as the virtual source with all source panels used for summing. Linear tapering is applied at the end traces in the correlation gather to attenuate the artifacts caused by edge effects. Apart from the direct arrivals, reflection events (shown by the arrows) are clear for both the causal and acausal responses. Note that the time scale is different than in the previous figure.

the correlation gather or sum the correlation gather over a larger source aperture. The virtual-source gather (Figure 20) generated after applying a linear taper to the correlation gather diminishes the edge effect.

If, instead of only summing over sources in source panel 5, all the sources are used for summing, the resulting virtual-source gather (Figure 21) forms an “X” shape with two linear events intersecting at time $t=0$ that correspond to the direct arrivals for both negative and positive offsets (with respect to receiver 60) and times. By using a larger source aperture, waves arrive at the virtual source from a larger range of directions, and, hence, the reflections at ± 1.3 s are present for both the negative and positive offsets. Using a larger source aperture also suppresses the artifacts caused by smaller source aperture (A in Figure 18) and the edge effect (C in Figure 18).

Summary. The acquisition geometry requirements for generating a virtual-source gather include specification of maximum allowable source spacing using a correlation gather and its f - k plot. Synthetic modeling allows estimation of a nonaliased virtual source. While summing the correlation gather, the nonzero contribution comes from the source location where the correlation gather timing peaks (stationary phase). Therefore, the choice of sources used for summing the correlation gather depends on the reference receiver (virtual source) location. Along with the source-spacing analysis, we can synthetically model this dependence before acquiring the field data. Use of the Mars Field OBC data showed that the traveltime difference curve can diagnose the shape of the edge effect, and tapering the ends of the correlation gather can practically suppress the edge effect.

Suggested reading. “The virtual source method: Theory and case study” by Bakulin and Calvert (GEOPHYSICS, 2006). “Seismic interferometry—Turning noise into signal” by Curtis et al. (TLE, 2006). “Interferometric/daylight seismic imaging” by Schuster et al. (*Geophysics Journal International*, 2004). “Extracting the Green’s function from the correlation of coda waves: A derivation based on stationary phase” by Snieder (*Physics Review E*, 2004). “Retrieving the elastodynamic Green’s function of an arbitrary inhomogeneous medium by cross-correlation” by Wapenaar (*Physics Review Letters*, 2004). “Spurious multiples in interferometric imaging of primaries” by Snieder et al. (GEOPHYSICS, 2006). “Retrieving the Green’s function by cross-correlation: A comparison of approaches” by Wapenaar et al. (*Journal of Acoustical Society of America*, 2005). “Correlation of random wavefields: An interdisciplinary review” by Larose et al. (GEOPHYSICS, 2006). “Improving the virtual source method using wavefield separation” by Mehta et al. (GEOPHYSICS, 2007a). “Virtual source method applied to Mars OBC data for time-lapse monitoring” by Mehta et al. (GEOPHYSICS, 2007b). “Continuation of wavefields in exploration seismology (Prodolzhenic volnovykh polei v zadachach Seismorazvedki)” by Petrashen and Nakhamkin (*Nauka*, 1973). **TJE**

Acknowledgments: We thank Shell for the financial support through the GameChanger Program and the permission to show the Mars Field OBC data. We appreciate the critical comments from Steve Hill to refine the article.

Corresponding author: kurangmehta@gmail.com